Reactivity of cobalt(II)-dichalcogenide complexes: correlation between redox conversion and ligand-field strength

Marvelous, C.

Chapter 2

Probing The Redox-conversion of Co(II)-disulfide to Co(III)-thiolate Complexes: The Effect of Ligand-Field Strength

*The redox-conversion reaction of cobalt(II)-disulfide to cobalt(III)-thiolate complexes triggered by addition of the bidentate ligand 2,2'-bipyridine (bpy) has been investigated. Reaction of the cobalt(II)-disulfide complex $[Co_2(L^1SSL^1)(X)_4]$ (L^1SSL^1 = di-2-(bis(2-pyridylmethyl)amino)-ethyldisulfide; X = Cl or Br) **[1X]** with 2,2'-bipyridine resulted in the formation of two different products, namely the cobalt(III)-thiolate complex $[Co(L^1S)(bpy)]X_2$ and the unexpected side product $[Co_2(L^1SSL^1)(bpy)_2(X)_2]X_2$. Crystals of $[Co_2(L^1SSL^1)(bpy)_2(Cl)_2](BPh_4)_2$ **[2Cl]**$(BPh_4)_2$ obtained after anion exchange showed the cobalt(II) ions to be in octahedral geometries with the nitrogen donors of the disulfide ligand arranged in a facial conformation and the chloride ion trans to the tertiary amine nitrogen. Remarkably, this side product cannot be converted to the cobalt(III)-thiolate compound $[Co(L^1S)(bpy)](SbF_6)_2$ **[3]**$(SbF_6)_2$ by removal of the chloride ion with use of a silver salt, as this causes scrambling of the ligands, resulting in the formation of $[Co(bpy)_3]^{n+}$. $[Co(L^1S)(bpy)](SbF_6)_2$ was obtained in a pure form by addition of bpy to a solution in acetonitrile of the compound $[Co(L^1S)(MeCN)_2]^{2+}$ **[4]**$^{2+}$. Addition of NEt_4Cl to **[3]**$(SbF_6)_2$ regenerates the cobalt(II)-disulfide complex **[1Cl]** as confirmed spectroscopically. DFT studies revealed that the conversion from **[1Cl]** to **[3]**$^{2+}$ most likely occurs via the hypothetical intermediate species **[2Cl]**$^{2+}_{mer}$, in which the nitrogen atoms of the disulfide ligand are arranged in a meridional conformation. Interestingly, the calculated d-orbital splitting energy of **[3]**$^{2+}$ is lower than that of **[4]**$^{2+}$, indicating that the ligand-field strength of bpy is lower than anticipated, which hampers clean conversion in the redox-conversion reaction. This study shows that the redox-conversion reaction between cobalt(II)-disulfide and cobalt(III)-thiolate complexes is intricate rather than straightforward.*

This chapter has been published as a full article: Christian Marvelous, Lucas de Azevedo Santos, Maxime A. Siegler, Célia Fonseca Guerra, and Elisabeth Bouwman, *Dalton Transactions,* 2022, **51**, 8046-8055.

2.1. Introduction

Thiol groups are involved in many important aspects of biological systems, notably in proteins as a cysteine amino acid residue, but also in cofactors.[1-3] Thiol groups have rich chemistry, the most known is its oxidation to disulfide species (S–S). The redox reaction of disulfide groups and thiolate ions is also prominent in enzymes, such as in glutathione reductase (glutaredoxin) that catalyzes the reduction of glutathione disulfide (GSSG) into glutathione (GSH).[4, 5] Such redox reactions in enzymes are often accompanied by a redox reaction of a metal center in the active site. However, it is challenging to study the mechanism of the redox-conversion in enzymes, due to the complexity of these systems.

In recent years, a number of studies focused on the thiol/disulfide redox-conversion reaction by making use of biomimetic metal-disulfide and metal-thiolate complexes.[6-14] The observation that the use of disulfide ligands in combination with copper(I) salts could lead to either copper(I)-disulfide or copper(II)-thiolate complexes was first reported by the group of Itoh about two decades ago.[14] Subsequently, it was reported that the redox-conversion reaction between copper(I)-disulfide and copper(II)-thiolate complexes is not only dependent on the ligand structure, but can be triggered by variations in anions, temperature, solvents, and the presence or absence of protons.[6-9] The group of Duboc was the first to report redox-conversion between cobalt(II)-disulfide and cobalt(III)-thiolate compounds, in which the presence or absence of halide ions determine the product of the reaction.[10] They reported a mononuclear, 5-coordinated cobalt(III)-dithiolate complex that upon removal of the chloride anion undergoes redox-conversion to form a dinuclear bis(μ-thiolato)dicobalt(II)-disulfide complex. Recently, our group reported the reversible redox-conversion between the mononuclear, 6-coordinated cobalt(III)-thiolate complex $[Co(L^1S)(MeCN)_2]^{2+}$ $[\mathbf{4}]^{2+}$ and the dinuclear cobalt(II)-disulfide complex $[Co_2(L^1SSL^1)Cl_4]$, as shown in **Scheme 2.1**.[15] In contrast to the system reported by Duboc's group, in our system *removal* of the chloride ions from the Co(II)-disulfide compound in acetonitrile results in the formation of the related Co(III)-thiolate compound. In order to understand the underlying mechanism in the redox-conversion reactions of Co(II)-disulfide and Co(III)-thiolate complexes these different outcomes have to be rationalized, even though they concern different systems.

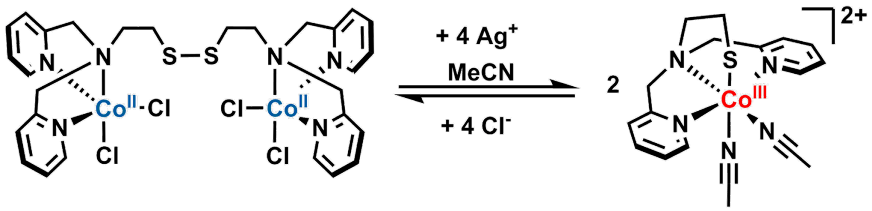

Scheme 2.1. Schematic representation of the reversible redox-conversion of the cobalt(II)-disulfide complex $[Co_2(L^1SSL^1)Cl_4]$ ([**1**$_{Cl}$]) and the cobalt(III)-thiolate complex $[Co(L^1S)(MeCN)_2]^{2+}$ ([**4**]$^{2+}$) induced by removal or addition of halide ions in MeCN solution.[15]

Our investigation is set out based on the observations described in our previous reports. The redox-conversion between cobalt(II)-disulfide and the corresponding cobalt(III)-thiolate complexes appears to be very sensitive to small changes. In the system that we reported earlier, conversion from the cobalt(II) to the cobalt(III) compound was induced by removing the chloride ions in an acetonitrile solution, or by the use of the thiocyanate anion. It is known that both acetonitrile and thiocyanate induce a stronger ligand-field effect than the π-donating chloride ion. The *d*-orbital splitting of the octahedral Co(III) ion is known to be larger than that of the Co(II) ion.[16, 17] Therefore, addition of a ligand that induces a stronger ligand-field effect to a Co(II) complex may yield an intermediate with a larger *d*-orbital splitting (**Figure 2.1**). When the ligand-field splitting is large enough to overcome the spin-pairing

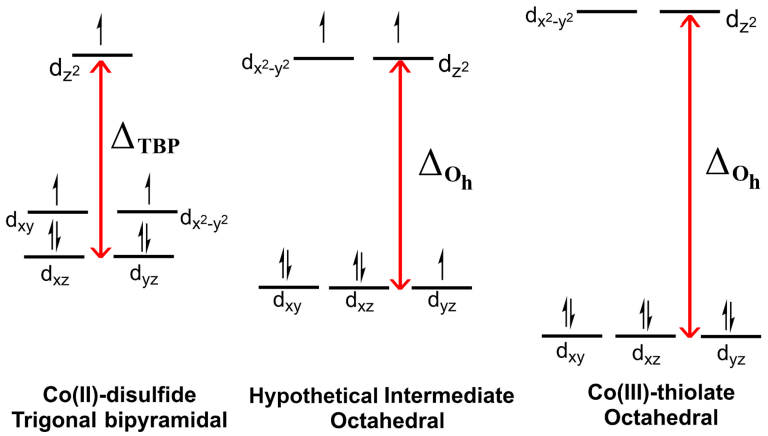

Figure 2.1. Energy diagrams of *d*-orbital splitting in Co(II)-disulfide and Co(III)-thiolate complexes.

energy, this results in a low-spin (LS) state for the Co(II) center. The instability of the high-energy single electron(s) in the Co(II) center may cause an electron transfer to the disulfide group, driving the reaction to form the cobalt(III)-thiolate species. Based on this theory, we suspect that addition of a ligand with a relatively large ligand-field strength will result in the formation of a Co(III)-thiolate species. Hence, in this study we report our investigation in the utilization of the relatively strong ligand-field, exogenous bidentate ligand 2,2'-bipyridine (bpy) to induce the redox-conversion from cobalt(II)-disulfide to cobalt(III)-thiolate species.

2.2. Results

2.2.1. Synthesis and Reactivity of the Cobalt Compounds

The cobalt(II)-disulfide compounds[$Co_2(L^1SSL^1)(X)_4$] [**1**$_X$] (X = Cl or Br) were prepared as depicted in **Scheme 2.2**.[14] Addition of the anhydrous $CoCl_2$ or $CoBr_2$ salt to a solution of L^1SSL^1 in either acetonitrile or methanol afforded solutions of the cobalt(II)-disulfide compounds [**1**$_{Cl}$] and [**1**$_{Br}$], respectively. The compounds were isolated as a purple powder for [**1**$_{Cl}$] in 89% yield and a light purple powder for [**1**$_{Br}$] in 60% yield. The compounds were obtained analytically pure as confirmed with elemental analysis. Unfortunately, the compounds described in this chapter appear to be rather labile; despite the use of analytically pure compounds the MS spectra often show multiple peaks indicating decomposition caused

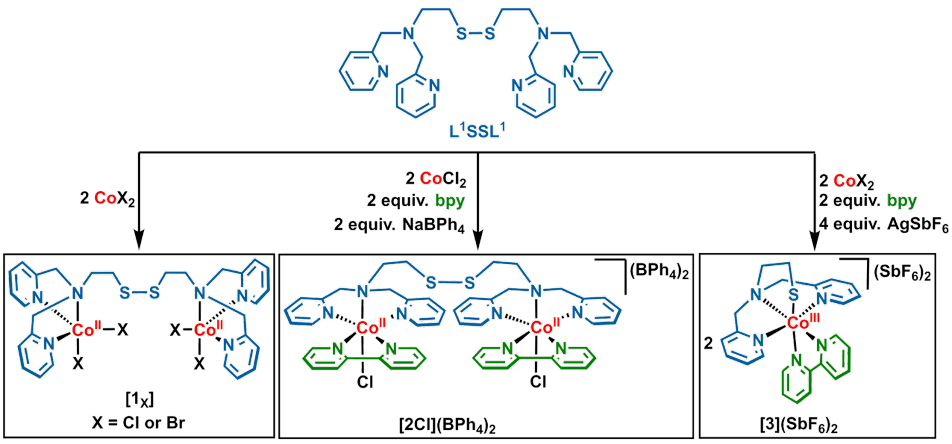

Scheme 2.2. Schematic overview of the synthetic procedures for the cobalt compounds of L^1SSL^1 described in the present work.

by the ionization conditions of ESI-MS. ESI-MS spectra of [$\mathbf{1}_{\mathbf{Cl}}$] dissolved in acetonitrile show peaks at *m/z* 352.0, 741.0, and 749.0 corresponding to the species [$\mathbf{1}_{\mathbf{Cl}}$ – $2Cl^-$]$^{2+}$, [$\mathbf{1}_{\mathbf{Cl}}$ – Cl^-]$^+$, [$\mathbf{1}_{\mathbf{Cl}}$ – $2Cl^-$ + $HCOO^-$]$^+$ (the formate ion arising from formic acid in the eluting solvent), respectively (Figure AI.1). Similar results were found in the ESI-MS spectra of [$\mathbf{1}_{\mathbf{Br}}$] (Figure AI.2), with peaks at *m/z* 398.0, 839.0, and 872.9 corresponding to the species [$\mathbf{1}_{\mathbf{Br}}$ – $2Br^-$]$^{2+}$, [$\mathbf{1}_{\mathbf{Br}}$ – $2Br^-$ + $HCOO^-$]$^+$, and [$\mathbf{1}_{\mathbf{Br}}$ – Br^-]$^+$, respectively. The cobalt(II)-disulfide compounds are paramagnetic, as indicated by the large shifts of the signals in their ^{1}H-NMR spectra up to 81 ppm (Figure AI.3−AI.4). The values of the magnetic moments in solution were estimated by Evans' method. The values of the magnetic moment of [$\mathbf{1}_{\mathbf{Cl}}$] and [$\mathbf{1}_{\mathbf{Br}}$] dissolved in DMSO-d_6 are 4.55 μ_B and 4.62 μ_B, respectively, calculated per cobalt center. Further characterization with a magnetic-susceptibility balance revealed their magnetic moment values in the solid state to be 4.38 μ_B and 4.35 μ_B per cobalt center for [$\mathbf{1}_{\mathbf{Cl}}$] and [$\mathbf{1}_{\mathbf{Br}}$], respectively. The magnetic moments of the compounds [$\mathbf{1}_{\mathbf{X}}$] are in agreement with the presence of two magnetically non-interacting high-spin Co(II) centers in the dinuclear molecules.

Dissolution of compound [$\mathbf{1}_{\mathbf{X}}$] in acetonitrile gives purple-colored solutions. Addition of two equivalents of bpy to this solution resulted in a color change to yellow, which was monitored using UV-visible spectroscopy. The UV-visible spectrum of compound [$\mathbf{1}_{\mathbf{Cl}}$] in acetonitrile is in agreement with the earlier report (**Figure 2.2**).[15] In contrast, the UV-visible spectrum of the yellow solution obtained after addition of bpy does not show clear absorption peaks in the visible region, indicating formation of cobalt(III) species in a low-spin (LS) electron configuration. Attempts at isolation of the anticipated cobalt(III)-thiolate compound $[Co(L^1S)(bpy)_2]Cl_2$ ([**3**]Cl_2) from the yellow solution resulted in a mixture of beige and red-colored powders, indicating the formation of at least two different products. Separation of these two products appeared to be difficult, and therefore [$\mathbf{1}_{\mathbf{Br}}$] was used in reactions with bipyridine with the hope that this would react more cleanly and yield the expected cobalt(III)-thiolate compound [**3**]$^{2+}$ in a pure form. Unfortunately, these reactions yielded similar results: workup after the reactions also led to mixtures of beige and red-colored powders, which again could not be separated.

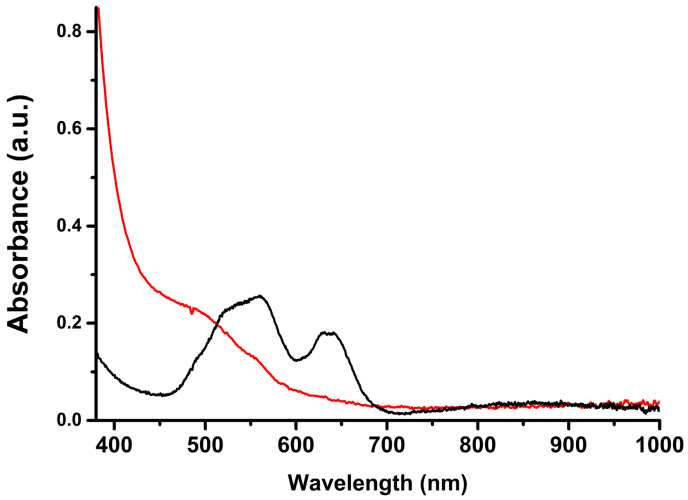

Figure 2.2. UV-Visible spectra of a purple solution of 5 mM [**1**$_{Cl}$] dissolved in acetonitrile (black line) and the yellow solution (red line) obtained after addition of 2 equivalents of 2,2'-bipyridine. UV-visible spectra were recorded using a transmission dip-probe with path length of 4 mm.

In attempts to clarify the composition of the mixtures, we performed different reactions. Reaction of [**1**$_{Cl}$] in methanol with two equivalents of bpy and with the addition of two equivalents of sodium tetraphenylborate resulted in the formation of the compound $[Co_2(L^1SSL^1)(bpy)_2(Cl)_2](BPh_4)_2$ ([**2**$_{Cl}$]$(BPh_4)_2$) as a beige powder after recrystallization in acetone (47% yield). ESI-MS spectra (Figure AI.5) show a peak at *m/z* 506.5 corresponding to the species $[\mathbf{2}_{Cl} - Cl^- + OMe^-]^{2+}$ (calculated *m/z* 506.1) and at 1011.9 corresponding to a partially reduced species $[\mathbf{2}_{Cl} - Cl^- + OMe^-]^{+}$ (calculated *m/z* 1012.2); this reduction possibly occurs during the ionization process. A peak at *m/z* 157.2 indicates the presence of free bpy. The magnetic susceptibility of [**2**$_{Cl}$]$(BPh_4)_2$ dissolved in DMSO-d_6 was measured using Evans' method, yielding a value of 4.12 μ_B calculated per cobalt center. This value suggests that the two cobalt(II) centers are most likely high-spin. Compound [**2**$_{Cl}$]$(BPh_4)_2$ was obtained analytically pure as shown by elemental analysis and the structure was determined using X-ray single crystal diffraction.

In another reaction in acetonitrile, the halide ions in [**1**$_{Cl}$] or [**1**$_{Br}$] were removed using four equivalents of silver hexafluoridoantimonate after which two equivalents of bpy were added. It is known that removal of the halide ions of [**1**$_{Cl}$] in acetonitrile yields the species $[\mathbf{4}]^{2+}$, and

subsequent addition of bpy resulted in the formation of [**3**]$(SbF_6)_2$, which was isolated as a dark red powder with variable yield of 68-93%. Elemental analysis of the bulk material demonstrates that [**3**]$(SbF_6)_2$ was obtained as an analytically pure compound. Interestingly, dissolution of the dark red powder in either acetonitrile or CD_3CN resulted in a dark red solution which in a few minutes turned light yellow, indicating instability of [**3**]$(SbF_6)_2$ in acetonitrile. The ^{1}H-NMR spectrum of [**3**]$(SbF_6)_2$ in CD_3CN (Figure AI.7) shows signals in the diamagnetic region as expected for low-spin Co(III) ions. However, the spectrum also shows that the compound [**3**]$(SbF_6)_2$ is not stable in solution; the aromatic peaks can be attributed to originate from [**3**]$(SbF_6)_2$, as well as $[\mathbf{4}]^{2+}$ and free bpy. ESI-MS spectra of [**3**]$(SbF_6)_2$ in acetonitrile (Figure AI.8) show the parent peak at *m/z* 708.0 corresponding to $[\mathbf{3}+SbF_6]^+$ (calculated *m/z* 708.0) and a dominant peak is found at 236.6 corresponding to the species $[\mathbf{3}]^{2+}$ (calculated *m/z* 236.55). In addition, the presence of $[\mathbf{4}]^{2+}$ is confirmed by a peak at *m/z* 199.6 (calculated *m/z* 199.55), and a peak at *m/z* 157.2 indicates the presence of free bpy. The magnetic susceptibility of compound [**3**]$(SbF_6)_2$ was measured in the solid state using a magnetic-susceptibility balance and in solution using Evans' method; both methods show that [**3**]$(SbF_6)_2$ is diamagnetic. Attempts were undertaken to obtain single crystals of compound $[\mathbf{3}]^{2+}$ using several counter anions, namely with SbF_6^-, PF_6^-, NO_3^-, BPh_4^-, BF_4^-, ClO_4^-, and $CF_3SO_3^-$. Unfortunately, these attempts were not successful or resulted in crystals that did not diffract well, which likely is related to the limited stability of the compound in solution.

After isolation and characterization of the pure compounds [$\mathbf{2}_{Cl}$]$(BPh_4)_2$ and [**3**]$(SbF_6)_2$ via the synthetic routes described above, we came to the conclusion that the beige and red-colored powders obtained from the reaction of [**1X**] with two equivalents of bpy correspond to the cobalt(II)-disulfide-bipyridine compound [**2X**]X_2 and the cobalt(III)-thiolate-bipyridine complex [**3**]X_2, respectively.

As [**1X**] upon reaction with bpy does not cleanly convert to $[\mathbf{3}]^{2+}$ we also attempted to convert [$\mathbf{2}_{Cl}$]$(BPh_4)_2$ to $[\mathbf{3}]^{2+}$ by removal of the chloride ions. The light brown solution of [$\mathbf{2}_{Cl}$]$(BPh_4)_2$ in acetonitrile or methanol immediately turned cloudy upon addition of two equivalents of $AgSbF_6$, indicating successful removal of the coordinated chloride anions. Further workup of the reaction mixture afforded a brown-reddish powder. Unexpectedly, ESI-MS of this powder dissolved in acetonitrile showed the presence of the species $[Co(bpy)_3]^{2+}$ (calcd.

m/z 263.57, found *m/z* 263.6) instead of the desired $[\mathbf{3}]^{2+}$ (Figure AI.9). The presence of the free ligand L^1SSL^1 is not detected, but several unidentified peaks are also present.

We then conducted a titration experiment to study whether the reverse reaction can be triggered with the addition of chloride ions. A solution of $[\mathbf{3}](SbF_6)_2$ in acetonitrile was titrated with a solution of tetraethylammonium chloride in acetonitrile (**Figure 2.3**). The addition of NEt_4Cl to the solution of $[\mathbf{3}](SbF_6)_2$ results in a color change of the solution from yellow to darker yellow, and some turbidity is observed. The UV-visible spectra show the decrease in absorbance of the peaks at 394 and 458 nm, and the appearance of new peaks at 565 and 642 nm upon addition of two equivalents of NEt_4Cl per $[\mathbf{3}]^{2+}$. The bands at 565 and 642 nm coincide with those of $[\mathbf{1}_{Cl}]$ in acetonitrile, indicating the formation of $[\mathbf{1}_{Cl}]$. Workup of the reaction mixture indeed resulted in the purple powder of $[\mathbf{1}_{Cl}]$, in a yield of 26%, as confirmed by the ESI-MS and ^{1}H-NMR spectra (Figure AI.10 and AI.11).

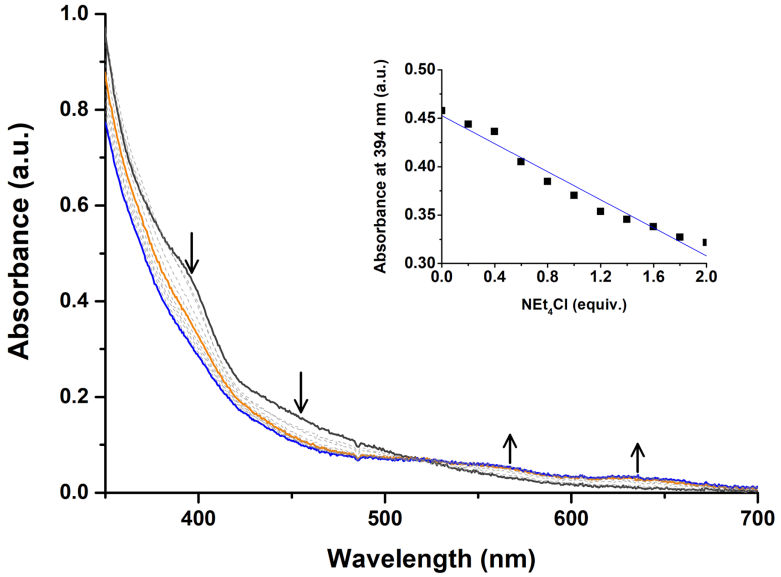

Figure 2.3. Changes of the UV-visible spectrum of 5 mM $[\mathbf{3}](SbF_6)_2$ in acetonitrile (black line) upon addition of NEt_4Cl (orange line = 1 equivalent, blue line = 2 equivalents). Inset shows the change of absorbance at 394 nm as a function of the amount of added NEt_4Cl. More details and change of absorbance at 458 nm are provided in Figure S12. UV-visible spectra were recorded using a transmission dip probe with 4 mm path length.

With the aim to confirm the assignment of $[\mathbf{3}]^{2+}$ being a cobalt(III)-thiolate compound, additional experiments were performed using 1,10-phenanthroline (phen) instead of bpy, as this ligand is structurally and electronically similar to bpy, but is less likely to dissociate due to its rigidity (See Supporting Information). ESI-MS spectra of an acetonitrile solution containing compound $[Co(L^1S)(phen)](SbF_6)_2$ (Figure AI.13) show peaks at *m/z* 732.0 and 248.6, corresponding to the species $[Co(L^1S)(phen)](SbF_6)^+$ (calculated *m/z* 732.0) and $[Co(L^1S)(phen)]^{2+}$ (calculated *m/z* 248.6), respectively. The species $[Co(phen)_3]^{2+}$ is also detected in the ESI-MS spectra at m/z 299.9 (calculated *m/z* 299.6). Crystallization attempts for $[Co(L^1S)(phen)](SbF_6)_2$ unfortunately resulted in crystals of the oxidized compound $[Co(L^1SO_2)(phen)](SbF_6)_2$ containing a sulfinate group (Figure AI.14 and Table AI.1).

2.2.2. Description of the Crystal Structures

The crystal structure of $[\mathbf{1}_{Cl}]$ was previously reported by our group.[15] The crystal data and refinement details for $[\mathbf{1}_{Br}]$ and $[\mathbf{2}_{Cl}](BPh_4)_2$ are provided in Table AI.2. The crystal structure of $[\mathbf{1}_{Br}]$ is similar to that of $[\mathbf{1}_{Cl}]$, but the compounds are not isostructural. $[\mathbf{1}_{Br}]$ crystallizes in the monoclinic space group $P2_1/c$. A projection of the structure of $[\mathbf{1}_{Br}]$ is depicted in **Figure 2.4.a**. A selection of bond distances and angles is provided in **Table 2.1**. In the asymmetric unit, one molecule of $[\mathbf{1}_{Br}]$ and one lattice methanol solvent molecule are co-crystallized. The distances and angles around the two independent cobalt centers are very similar. Similar to $[\mathbf{1}_{Cl}]$, each cobalt center in $[\mathbf{1}_{Br}]$ is coordinated to three nitrogen atoms of

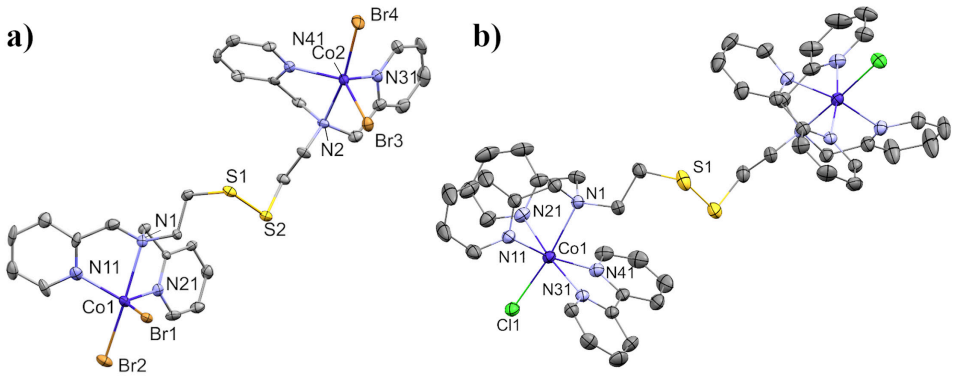

Figure 2.4. Displacements ellipsoid plots (50% probability level) of a) $[Co_2(L^1SSL^1)(Br)_4]$ ($[\mathbf{1}_{Br}]$) and b) $[Co_2(L^1SSL^1)(bpy)_2(Cl)_2]^{2+}$ ($[\mathbf{2}_{Cl}]^{2+}$) at 110(2) K. Hydrogen atoms, non-coordinated anions, and lattice solvent molecules are omitted for clarity.

Table 2.1. Selected bond distances and bond angles in [$\mathbf{1}_{\mathbf{Br}}$].

Atoms	distance (Å)	Atoms	Bond angles (°)
Co1–Br1	2.4589(9)	Br1−Co1−Br2	99.92(3)
Co1–Br2	2.4613(9)	Br1−Co1−N1	90.13(10)
Co1–N1	2.350(4)	Br1−Co1−N11	110.58(13)
Co1–N11	2.074(5)	Br1−Co1−N21	123.75(13)
Co1–N21	2.071(4)	Br2−Co1−N1	169.76(11)
Co1–S1	6.037(1)	N11−Co1−N21	117.99(18)
S1–S2	2.036(2)	N11−Co1−N1	76.11(17)
Co1–Co2	11.671(1)	N21−Co1−N1	76.22(16)

the dinucleating ligand and two halide ions in a distorted trigonal-bipyramidal geometry, with τ_5 values of the two cobalt centers being 0.77 and 0.66.[18] One intermolecular interaction was found between Br4 and the OH group of the lattice methanol solvent molecule. Even though the structure of [$\mathbf{1}_{\mathbf{Br}}$] is similar to that of [$\mathbf{1}_{\mathbf{Cl}}$], the distance between the two cobalt centers in [$\mathbf{1}_{\mathbf{Br}}$] is significantly larger than in [$\mathbf{1}_{\mathbf{Cl}}$] (11.671 Å vs 8.160 Å).

A projection of the structure of [$\mathbf{2}_{\mathbf{Cl}}$](BPh_4)$_2$ is depicted in **Figure 2.4.b**. Selected bond distances and angles are provided in **Table 2.2**. [$\mathbf{2}_{\mathbf{Cl}}$](BPh_4)$_2$ crystallizes in the monoclinic space group *C*2/*c*. The asymmetric unit contains one half of the dinuclear complex found at a site of twofold axial symmetry, one tetraphenylborate anion, one lattice acetone solvent molecule, and one partially occupied lattice water molecule (found at a site of twofold axial symmetry). Both cobalt centers are in a distorted octahedral geometry, coordinated with five nitrogen donor atoms (three from L^1SSL^1 and two from bpy) as well as one chloride ion. The three nitrogen donor atoms from the ligand L^1SSL^1 are arranged in a facial fashion, with the

Table 2.2. Selected bond distances and angles in [$\mathbf{2}_{\mathbf{Cl}}$](BPh_4)$_2$.

Atoms	Distance (Å)	Atoms	Bond angles (°)
Co1−Cl1	2.3827(6)	N1−Co1−Cl1	171.79(4)
Co1−N1	2.2579(15)	N1−Co1−N11	79.53(6)
Co1−N11	2.1430(16)	N1−Co1−N21	77.32(6)
Co1−N21	2.1394(16)	N1−Co1−N31	97.58(6)
Co1−N31	2.1337(15)	N1−Co1−N41	90.41(6)
Co1−N41	2.1260(16)	Cl1−Co1−N11	97.42(5)
Co1−Co1’	11.6516(9)	Cl1−Co1−N21	94.79(5)
Co1−S1	5.8773(9)	Cl1−Co1-N31	90.46(4)
S1-S1’	2.0298(12)	Cl1-Co1-N41	93.03(5)
		N11−Co1−N21	82.73(6)
		N11−Co1−N31	100.87(6)
		N41−Co1−N21	98.72(6)
		N41−Co1−N31	76.67(6)

tertiary amine nitrogen located *trans* to the chloride ion. The remaining positions are occupied by the two nitrogen donors from bpy.

The average length of the equatorial Co–N bonds is 2.14 Å, in agreement with the presence of high-spin cobalt(II) centers.[19-21] The Co–Cl bond length is slightly larger (2.38 Å) than in [**1**$_{Cl}$] (2.32 and 2.27 Å), indicating that the Co–Cl bond in [**2**$_{Cl}$]$(BPh_4)_2$ is slightly weaker. The distance between the cobalt center and the nearest disulfide sulfur atom is slightly smaller (5.88 Å) than those in [**1**$_{Cl}$] (5.96 Å and 5.93 Å). The intramolecular distance between two cobalt centers in [**2**$_{Cl}$]$(BPh_4)_2$ is similar to that in [**1**$_{Br}$].

2.2.3. Density Functional Theory Studies

Density Functional Theory (DFT) computations were performed in order to provide a rationale for the complication when bpy is used in a reaction with [**1**$_X$] to form [**3**]$^{2+}$, for which we optimized the geometries of several complexes. The dinuclear cobalt(II)-disulfide compound [**1**$_{Cl}$] was simplified to [**1***] in order to make a fair comparison with [**3**]$^{2+}$ as well as [**4**]$^{2+}$, i.e. the molecule is mononuclear. The molecule [**1***] comprises half of [**1**$_{Cl}$] with a methyl group on the tertiary amine nitrogen instead of the disulfide moiety (**Figure 2.5**). The cobalt(III)-thiolate compound [**3**]$^{2+}$ was optimized for two different geometries, differing in

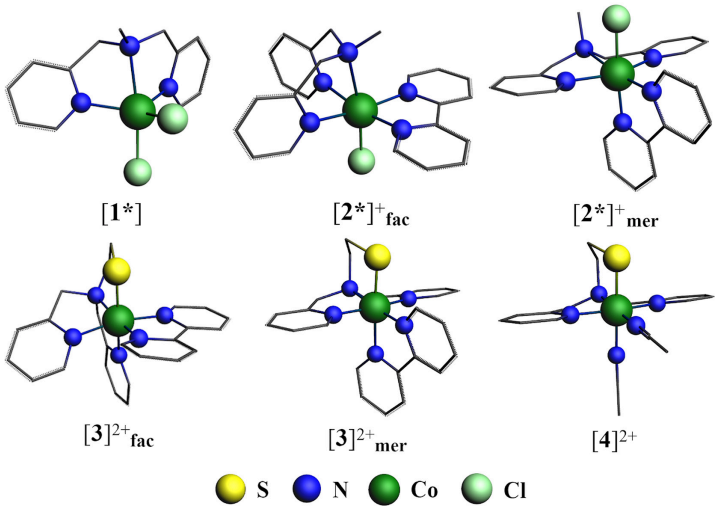

Figure 2.5. Optimized geometry structures of all calculated compounds. Carbon atoms are shown in wireframe and hydrogen atoms are omitted for clarity.

the binding mode of the three nitrogen donors of the ligand L^1S^- (**Figure 2.5**), being facial in $[\mathbf{3}]^{2+}_{fac}$ or meridional in $[\mathbf{3}]^{2+}_{mer}$; the latter orientation corresponds to the structure reported for $[\mathbf{4}]^{2+}$,[15] which was also computed to serve as a comparison for $[\mathbf{3}]^{2+}$. In addition, we were interested in finding out why the side product $[\mathbf{2}_{Cl}]$ cannot be converted into $[\mathbf{3}]^{2+}$ and therefore the side product $[\mathbf{2}_{Cl}]$ was simplified into $[\mathbf{2*}]^{+}_{fac}$, similar to [**1***]. We also considered the hypothetical isomeric compound $[\mathbf{2*}]^{+}_{mer}$, in which the nitrogen donors of the L^1 fragment are in a meridional conformation, similar to $[\mathbf{3}]^{2+}_{mer}$. Based on the experimental data, geometry optimization of [**1***], $[\mathbf{2*}]^{+}_{fac}$, $[\mathbf{2*}]^{+}_{mer}$ was done with $S = 3/2$ (for high-spin Co(II) complexes), while for $[\mathbf{3}]^{2+}_{fac}$, $[\mathbf{3}]^{2+}_{mer}$, and $[\mathbf{4}]^{2+}$ the optimization was done with $S = 0$ (low-spin Co(III) complexes).

The optimized geometries of the complexes are depicted in **Figure 2.5**. The simplified side product $[\mathbf{2*}]^{+}_{fac}$ is more stable by 5 kcal/mol than the hypothetical isomer $[\mathbf{2*}]^{+}_{mer}$. In addition, $[\mathbf{3}]^{2+}_{mer}$ is more stable than $[\mathbf{3}]^{2+}_{fac}$ by 8 kcal/mol and therefore $[\mathbf{3}]^{2+}_{mer}$ was used for further analyses. The likelihood that $[\mathbf{3}]^{2+}_{mer}$ corresponds with the actual structure of $[\mathbf{3}]^{2+}$ is supported by the crystal structure of $[Co(L^1SO_2)(phen)](SbF_6)_2$ (Figure AI.14) and $[\mathbf{4}](BF_4)_2$,[15] in which the nitrogen donors of L^1S^- are indeed arranged in a meridional fashion. The results obtained for $[\mathbf{4}]^{2+}$ in a low-spin (S=0) state are in agreement with the previous report.[15]

We then studied the energy levels of the molecular orbitals, with a focus on the MO's with large contributions of *d*-orbitals of the cobalt centers, with the aim to estimate the ligand-field splitting energies. The levels of the five molecular orbitals with largest contribution of the Co *d*-orbitals in [**1***], $[\mathbf{2*}]^{+}_{fac}$, $[\mathbf{2*}]^{+}_{mer}$, $[\mathbf{3}]^{2+}_{mer}$, and $[\mathbf{4}]^{2+}$ are shown in **Figure 2.6** (see Figures S15-S19 for detailed description). The MO's comprising large contribution of Co *d*-orbitals are not separated into two or three degenerated energy levels as expected for ideal geometries described by the ligand-field theory.[22] Instead, we found the cobalt *d*-orbitals to be distributed in five different energy levels, due to the asymmetry of the compounds. However, notably in the octahedral compounds it is clear that the *d*-orbitals are distributed into two sets of (nearly degenerate) energy levels, qualitatively corresponding to the t_{2g} and e_g levels defined by ligand-field theory.

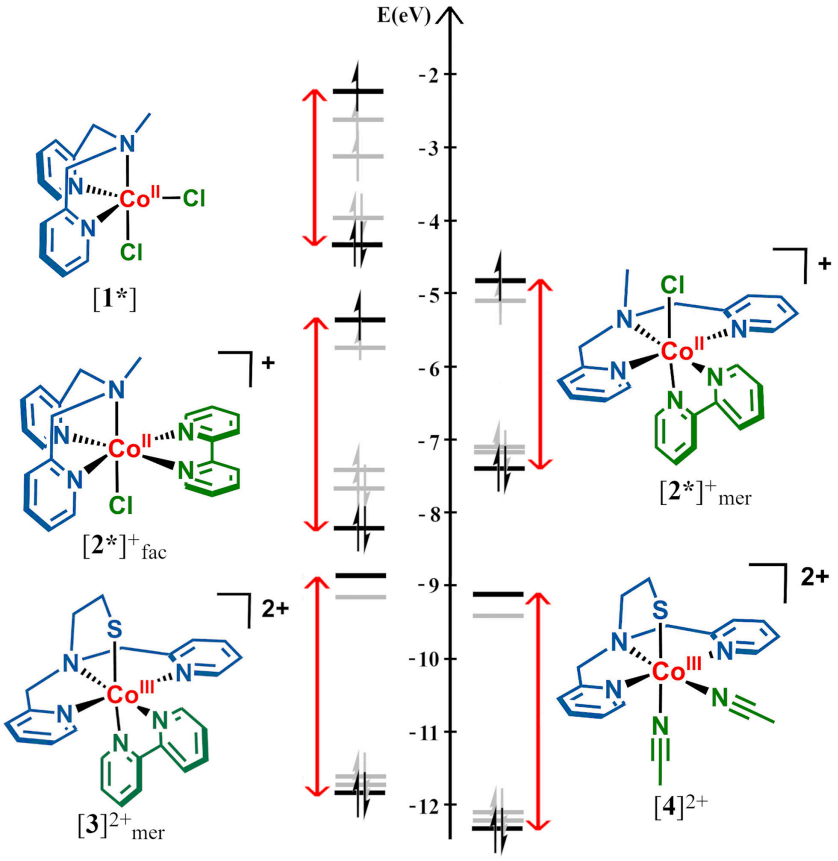

Figure 2.6. Simplified energy level diagrams for [**1***], [**2***]$^{+}_{fac}$, [**2***]$^{+}_{mer}$, [**3**]$^{2+}_{mer}$, and [**4**]$^{2+}$. Molecular orbital diagrams show only the five energy levels with the largest Co *d*-orbital contributions (highest-lying and lowest-lying energy levels are denoted in black, the remaining energy levels are denoted in grey). The three colors used in the structures indicate the fragments that were used in the DFT computations.

It is not possible to calculate the ligand-field splitting energies from the five molecular orbitals due to the non-degeneracy and the molecular orbitals being a mix of cobalt *d*-orbitals and ligand orbitals (see Figures S15-S19). Thus, we can discuss the energy differences in these MO's only in a qualitative way. The energy difference between the highest and lowest MO with large *d*-orbital contribution seems to be larger for [**2***]$^{+}_{fac}$ than for the hypothetical isomer [**2***]$^{+}_{mer}$. Furthermore, the energy difference in [**4**]$^{2+}$, containing two acetonitrile molecules, is slightly larger than that of the bpy-containing compound [**3**]$^{2+}_{mer}$. Our results thus indicate that for our system, bpy has lower ligand-field strength than acetonitrile, which

is in contradiction with the spectrochemical series.[17, 23-25] It has been reported that bpy might have similar or even larger π-donating than π-accepting properties, suggesting that the large ligand-field strength of bpy may be overestimated.[26]

Upon closer inspection of the distribution of the electron density and energy levels of the SOMOs of $[\mathbf{2^*}]^+_{fac}$ and $[\mathbf{2^*}]^+_{mer}$, we found some interesting differences. In $[\mathbf{2^*}]^+_{fac}$ the SOMO and the SOMO-1 are at –5.1 eV and −5.7 eV and have respectively mainly cobalt $d_{x^2-y^2}$ and d_{z^2} character, whereas in the hypothetical intermediate $[\mathbf{2^*}]^+_{mer}$ the SOMO and SOMO–1 are at –4.8 eV and−5.1 eV and have mainly cobalt d_{z^2} and $d_{x^2-y^2}$ character. Thus, the highest SOMO in $[\mathbf{2^*}]^+_{mer}$ is more destabilized than in $[\mathbf{2^*}]^+_{fac}$ and consequently, the single electron from this SOMO will be transferred more readily from the Co(II) center to the disulfide sulfur atom in a redox-conversion reaction. More importantly, if the chloride ion leaves the cobalt in $[\mathbf{2^*}]^+_{fac}$ and $[\mathbf{2^*}]^+_{mer}$, respectively, the SOMO–1 and SOMO with the d_{z^2} character becomes available to the sulfur atom. From **Figure 2.7**, it is clear that the SOMO in $[\mathbf{2^*}]^+_{mer}$ can be more readily approached by a sulfur atom of the disulfide group. In contrast, in $[\mathbf{2^*}]^+_{fac}$ extensive rearrangements are necessary to make the d_{z^2} orbital available to the sulfur atom in order to produce the $[\mathbf{3}]^{2+}_{fac}$.

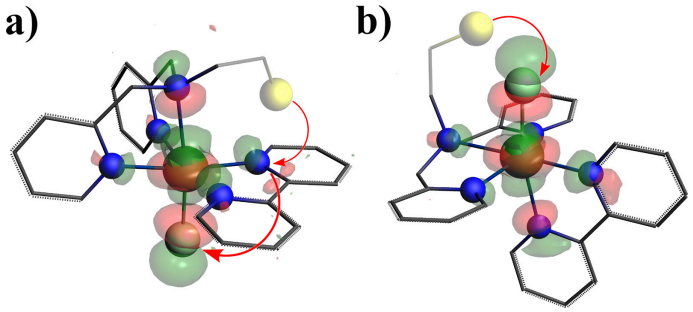

Figure 2.7. Schematic drawings of the approach of the sulfur atom to replace chloride in a) $[\mathbf{2^*}]^+_{fac}$ and b) $[\mathbf{2^*}]^+_{mer}$. The d_{z^2} character of $[\mathbf{2^*}]^+_{fac}$ and $[\mathbf{2^*}]^+_{mer}$ (SOMO−1 and SOMO, respectively) is shown as orbital lobes. The sulfur atom was omitted in the calculation of $[\mathbf{2^*}]^+_{fac}$ and $[\mathbf{2^*}]^+_{mer}$, but is included for clarity.

2.3. Discussion

It has been reported that redox-conversion reactions of cobalt(II)-disulfide complexes to the corresponding cobalt(III)-thiolate complexes occur under certain conditions.[10, 13, 15] We reported that removal of the chloride ions from [**1**$_{Cl}$] in acetonitrile leads to the formation of [**4**]$^{2+}$, whereas in methanol the compound remains in the cobalt(II)-disulfide state.[15] Furthermore, the reaction of L^1SSL^1 with $Co(NCS)_2$ in acetonitrile as well as methanol or dichloromethane leads to the immediate formation of $[Co(L^1S)(NCS)_2]$.[15, 27] As both acetonitrile (MeCN) and the thiocyanate anion ($[NCS]^-$) are ligands with a stronger ligand-field effect than that of the chloride ion, we hypothesized that the initial formation of a low-spin Co(II)-disulfide intermediate with two degenerate, high-energy MOs containing a single electron facilitates the redox-conversion by electron transfer to the disulfide group.

We assumed that bpy would trigger the redox-conversion reaction of cobalt(II)-disulfide [**1**X] to the cobalt(III)-thiolate compound [**3**]$^{2+}$, possibly without the need to remove the halide ions, as bpy is a chelating ligand that is reported to have a relatively strong ligand-field effect. Our initial spectroscopic studies suggested that this redox-conversion reaction indeed occurred, as indicated by the color change of the solution and the change in the UV-Vis spectrum upon addition of two equivalents of bpy to a solution of [**1**X] (See **Scheme 2.3**, reaction I). However, it appeared that full conversion of [**1**X] to [**3**]$^{2+}$ does not take place; workup showed that a mixture is formed of [**3**]$^{2+}$ and [**2**X]$^{2+}$. Unexpectedly, formation of [**3**]$^{2+}$ by halide abstraction of [**2**X]$^{2+}$ (**Scheme 2.3**, reaction II) was unsuccessful, as this reaction led to the formation of $[Co(bpy)_3]^{2+}$.

Removal of the halides of [**1**X] in acetonitrile leads to the formation of [**4**]$^{2+}$ (**Scheme 2.3**, reaction III); subsequent addition of bpy results in replacement of the solvent molecules forming [**3**]$^{2+}_{mer}$ (**Scheme 2.3**, reaction IV). In contrast to the reaction of [**1**X] with bpy (**Scheme 2.3**, reaction I), formation of [**4**]$^{2+}$ via removal of halides in acetonitrile (**Scheme 2.3**, reaction III) is clean;[15] it is most likely driven by the excess of acetonitrile (as solvent) as there is no other ligand present. In addition, [**3**]$(SbF_6)_2$ appeared to be unstable when dissolved in acetonitrile, possibly due to bpy having lower ligand-field strength than anticipated (**Scheme 2.3**, reaction V). Finally, we have shown that treatment of a solution of [**3**]$(SbF_6)_2$ with the chloride salt NEt_4Cl in acetonitrile (**Scheme 2.3**, reaction VI) leads to the formation of [**1**$_{Cl}$], indicating that the reverse reaction is indeed possible.

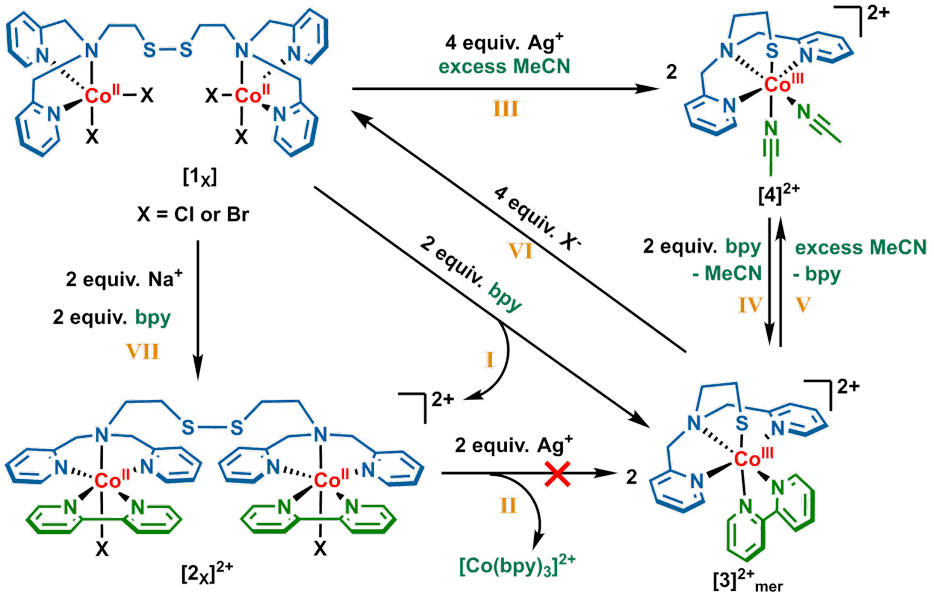

Scheme 2.3. Overview of all reactions described in this chapter.

The X-ray structure of $[\mathbf{2}_{Cl}](BPh_4)_2$ in combination with the molecular orbital analyses of $[\mathbf{2^*}]^+_{fac}$ and $[\mathbf{2^*}]^+_{mer}$ provide an explanation for our observations. Due to the facial orientation of the three nitrogen donors of the L^1 fragment in $[\mathbf{2}_{Cl}]^{2+}$, approach of the disulfide group to the SOMO−1 based on the d_{z^2} orbital of the cobalt center necessary for the electron transfer is hampered by the chelating bpy (**Figure 2.7.a**). Several donor atoms need to dissociate and move to other relative positions to allow for the generation of either $[\mathbf{3}]^{2+}_{fac}$ or $[\mathbf{3}]^{2+}_{mer}$. If during this process bpy dissociates, ligand scrambling leads to the formation of $[Co(bpy)_3]^{2+}$. The formation of $[Co(bpy)_3]^{2+}$ is favourable due to its high stability constant ($\log\beta_3 = 16.1$ in water with 0.1 M ionic strength, $\log\beta_3 = 36.08$ in 1,2-dichloroethane).[28, 29] We therefore could not use an excess bpy in our reactions to drive reaction I to completion.

In contrast, the coordination mode in the hypothetical intermediate $[\mathbf{2^*}]^+_{mer}$ allows approach of the disulfide group to the SOMO with high contribution of the cobalt d_{z^2} orbital, thus replacing the chloride ion (**Figure 2.7.b**). Thus, addition of bpy to [**1**x] can lead to two 'intermediates': the stable compound $[\mathbf{2}]^{2+}$ that is found as a 'by product' and a potentially unstable intermediate with the nitrogen atoms of the L^1 fragment in meridional positions (resembling $[\mathbf{2^*}]^+_{mer}$), which readily converts to $[\mathbf{3}]^{2+}$ and is thus not observed as a product.

2.4. Conclusion

The redox-conversion of cobalt(II)-disulfide compound [**1**$_{\mathbf{X}}$] to the cobalt(III)-thiolate complex [**3**]$^{2+}$ using the bidentate ligand bpy has been investigated using various spectroscopic methods as well as DFT calculations. The formation of species [**3**]$^{2+}$ from [**1**$_{\mathbf{X}}$] indicates that bpy is indeed able to induce the redox-conversion of a cobalt(II)-disulfide to a cobalt(III)-thiolate complex, even without the addition of silver salts to remove the chloride ions, although the formation of side product [**2**$_{\mathbf{X}}$]$^{2+}$ appeared to be inevitable. For the redox-conversion to occur starting from the intermediate [**2**$_{\mathbf{X}}$]$^{2+}$, reorganisation of the donor atoms at cobalt is necessary, and dissociation of bpy during this process results in the formation of highly stable tris–bipyridine cobalt compounds. Furthermore, our DFT studies show that the conversion from [**1**$_{\mathbf{Cl}}$] to [**3**]$^{2+}$ most likely proceeds via an intermediate in which the nitrogen atoms of the disulfide ligand are arranged in a meridional fashion, making it possible for the disulfide sulfur atom to approach the high-energy SOMO with predominant cobalt d_{z^2} contribution for electron transfer.

Our initial hypothesis that the redox-conversion of [**1**$_{\mathbf{X}}$] to a cobalt(III) thiolate compound may be induced simply by addition of a strong-field ligand thus has not yet been firmly proven. First of all, it turns out that the ligand-field splitting strength of bpy is lower than anticipated, and additionally, the use of bpy leads to the formation of the highly stable $[Co(bpy)_3]^{n+}$. Furthermore, the coordination mode of the ligands appear to be vital, as demonstrated by this study and our previous report. Further studies will be directed to the use of other ligands that are higher in the spectrochemical series, which may further corroborate our findings by inducing cleaner redox-conversion reactions of cobalt(II)-disulfide to the related cobalt(III)-thiolate complexes.

2.5. Experimental Section

2.5.1. General

All reagents were purchased from commercial sources and used as received unless noted otherwise. Degassed solvents used were obtained by the freeze-pump-thaw method followed by drying the solvents using the appropriate size of molecular sieves. The ligand L^1SSL^1 and cobalt compound $[Co_2(L^1SSL^1)Cl_4]$ [**1**$_{\mathbf{Cl}}$] were prepared according to previously published methods.[14, 15] The synthesis of the cobalt compounds was performed using standard

Schlenk-line techniques under argon atmosphere. ^{1}H NMR spectra were recorded on a Bruker 300 DPX spectrometer at room temperature. Mass spectra were recorded on a Thermo Scientific MSQ Plus mass spectrometer with electrospray ionization (ESI) method. Formic acid was added to the eluting solvent in a final concentration of 1% (v/v). Simulated mass spectra were generated using mMass (version 5.5.0) software.[30] IR spectra were obtained using a PerkinElmer Spectrum Two System equipped with Universal ATR module containing diamond crystal for single reflection (scan range 400–4000 cm^{-1}, resolution 4 cm^{-1}). UV-visible spectra were collected using a transmission dip probe with variable path lengths and a reflection probe on an Avantes AvaSpec-2048 spectrometer and using an Avalight-DH-S-Bal light source. Elemental analyses were performed by the Microanalytical Laboratory Kolbe in Germany.

2.5.2. Single crystal X-ray crystallography

All reflection intensities were measured at 110(2) K using a SuperNova diffractometer (equipped with Atlas detector) with Mo *K*α radiation (λ = 0.71073 Å) under the program CrysAlisPro (Version CrysAlisPro 1.171.39.29c, Rigaku OD, 2017). The same program was used to refine the cell dimensions and for data reduction. The structure was solved with the program SHELXS-2018/3 and was refined on F^2 with SHELXL-2018/3.[31] Numerical absorption correction based on Gaussian integration over a multifaceted crystal model was applied using CrysAlisPro. The temperature of the data collection was controlled using the system Cryojet (manufactured by Oxford Instruments). The H atoms were placed at calculated positions using the instructions AFIX 23, AFIX 43, AFIX 137 or AFIX 147 with isotropic displacement parameters having values 1.2 or 1.5 U_{eq} of the attached C or O atoms.

The structure of compound [$\mathbf{1}_{\mathbf{Br}}$] is partly disordered. The lattice methanol solvent molecule is found to be disordered over two orientations, with the occupancy factor of the major component of the disorder refining to 0.68(3). The H atoms H1OM and H1O' attached to O1S and O1S' (disordered MeOH lattice solvent molecule) were found from difference Fourier maps, and their coordinates were constrained to be the same using the EXYZ instruction. The O1S−H1OM and O1S'−H1O' bond distances were set to be refined pseudo-freely using the DFIX instruction in order to keep the O−H distance within an acceptable range.

For compound [**2**]$(BPh_4)_2$, the H atom attached to O1W (partially occupied lattice water molecule found at one site of twofold axial symmetry, occupancy factor: 0.419(11)) could not reliably retrieved from the difference Fourier map. The structure is partly disordered. One phenyl group and the lattice acetone solvent molecule are disordered over two orientations, and the occupancy factors of the major components of the disorder refine to 0.874(6) and 0.778(10), respectively. The asymmetric unit also contains another lattice solvent molecule (or a mixture of lattice solvent molecules) that is very disordered. While it might be one partially occupied disordered acetone lattice solvent molecule, it is difficult to assess with certainty the exact nature of the lattice solvent molecule. This contribution has been removed using the SQUEEZE procedure in Platon.[32, 33] The crystal structures of [$\mathbf{1}_{\mathbf{Br}}$], [$\mathbf{2}_{\mathbf{Cl}}$]$(BPh_4)_2$, and [Co(L^1SO_2)(phen)]$(SbF_6)_2$ can be accessed via Cambridge Crystallographic Data Center database, CCDC deposit number: 2093906, 2093907, 2093908.

2.5.3. DFT Calculations

All calculations were performed with the Amsterdam Density Functional (ADF) program version 2017.103.[34] Geometries and energies were computed using OPBE functional.[35] Molecular orbitals (MO) were expanded in a large uncontracted TZP Slater type orbital (STO) basis set.[36] Scalar relativistic effects were accounted for using the zeroth order regular approximation (ZORA).[37] The stationary points were checked to be minima at potential energy surface using vibrational analysis. The simplified compound [**1***], $[\mathbf{2}^*]^+_{fac}$, and $[\mathbf{2}^*]^+_{mer}$ were optimized with $S = 3/2$ (high-spin cobalt(II) center). For the compounds $[\mathbf{3}]^{2+}$ (both facial and meridional conformation) and $[\mathbf{4}]^{2+}$, calculations were done with $S = 0$ (low-spin cobalt(III) center).

2.5.4. Synthesis of the compounds

[$Co_2(L^1SSL^1)Br_4$] ([$\mathbf{1}_{\mathbf{Br}}$])

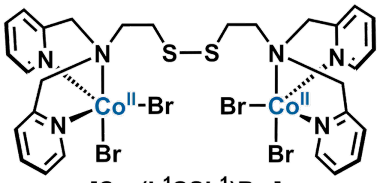

[$Co_2(L^1SSL^1)Br_4$]

The ligand L^1SSL^1 (129 mg, 0.25 mmol) was dissolved in 5 mL dry and degassed acetonitrile. Into the solution of the ligand, anhydrous $CoBr_2$ (109 mg, 0.50 mmol, 2 equiv.) was then added. The resulting purple solution was then stirred for 1 hour. The solution was then concentrated until approximately 1 mL was left in the flask. Into the flask, 12 mL dry and

degassed diethyl ether was added and immediately pale purple precipitates were formed. The precipitates were then washed twice with 10 mL dry and degassed diethyl ether, filtered, and then dried in vacuo. Yield: 144 mg, 0.151 mmol, 60%. Single crystals of [**1**$_{\mathbf{Br}}$] were grown after approximately a week using vapor diffusion of diethyl ether into a methanol solution of compound [**1**$_{\mathbf{Br}}$]. IR (neat, cm^{-1}): 1608s, 1571w, 1480m, 1445s, 1310m, 1291m, 1257w, 1155w, 1092m, 1054m, 1025s, 965w, 862m, 766s, 738m, 650m, 522w, 417m. ESI-MS calcd. for [**1**$_{\mathbf{Br}}$ – Br]$^{+}$ *m/z* 872.8, found *m/z* 872.9, calcd. for [**1**$_{\mathbf{Br}}$ – 2Br]$^{2+}$ *m/z* 398.0, found *m/z* 398.0. Elemental analysis (%) for [**1**$_{\mathbf{Br}}$]·0.6 H_2O, calcd. C, 34.85; H, 3.47; N, 8.71; found C, 34.89; H, 3.51; N, 8.70.

[Co$_2$(L^{1}SSL^1)(bpy)$_2$(Cl)$_2$](BPh$_4$)$_2$ ([2$_{Cl}$](BPh$_4$)$_2$)

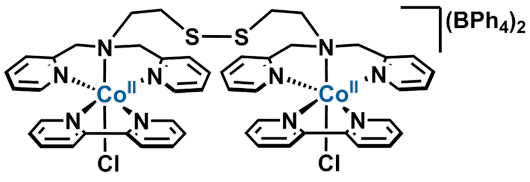

[Co$_2$(L^{1}SSL^1)(bpy)$_2$(Cl)$_2$](BPh$_4$)$_2$

Ligand L^{1}SSL^1 (52.01 mg, 0.1 mmol) was dissolved in 5 mL dry and degassed methanol. After all the ligand was dissolved, anhydrous $CoCl_2$ (26.21 mg, 0.2 mmol, 2 equiv.) was added to the solution, resulted in dark purple solution. The solution was stirred for 30 minutes, then 2,2'-bipyridine (31.43 mg, 0.2 mmol, 2 equiv.) was added and the solution color immediately turned orange. After stirring the solution for 2 hours, sodium tetraphenylborate (68.90 mg, 0.2 mmol, 2 equiv.) was added to remove 2 equiv. of chloride ligands. The addition of sodium tetraphenylborate quickly resulted in suspension. Into this suspension, 3 mL dry and degassed acetone was added to re-dissolve the complex. The suspension was then turned into solution again with small amount of white precipitates. The solution was filtered into a clean Schlenk flask, and then concentrated under reduced pressure until approximately 1 mL was left in the flask. Into the flask, 12 mL dry and degassed diethyl ether was then added, which afforded beige-colored precipitates. The precipitates were washed twice with 10 mL dry and degassed diethyl ether, filtered, and dried in vacuo. Yield: 78 mg, 47%. Single crystals suitable for X-ray diffraction for this compound were obtained by vapor diffusion of acetone into a methanol solution of [**2**](BPh$_4$)$_2$. IR (neat, cm^{-1}): 3050w, 1603m, 1477m, 1439m, 1314w, 1262w, 1156w, 1058w, 1018m, 766m, 732s, 704s, 611m. ESI-MS calcd. for [**2**$_{\mathbf{Cl}}$ – Cl^{-} + OMe^{-}]$^{2+}$ *m/z* 506.1, found *m/z* 506.5, calcd. for [**2**$_{\mathbf{Cl}}$ – Cl^{-} + OMe^{-}]$^{+}$ *m/z* 1012.2,

found *m/z* 1011.9. Elemental analysis (%) for [**2**$_{Cl}$](BPh$_4$)$_2$·2 H$_2$O, calcd. C, 68.13; H, 5.48; N, 8.28; found C, 68.13; H, 5.41; N, 8.27.

[Co(L^{1}S)(bpy)](SbF$_6$)$_2$ ([3](SbF$_6$)$_2$)

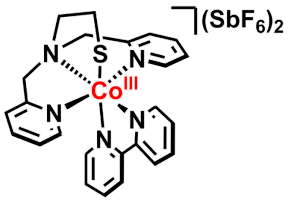

[Co(L^{1}S)(bpy)](SbF$_6$)$_2$

Ligand L^{1}SSL^1 (52.25 mg, 0.1 mmol) was dissolved in 5 mL dry and degassed acetonitrile. Into the solution of the ligand, anhydrous $CoBr_2$ (44.10 mg, 0.2 mmol, 2 equiv.) was added, resulted in a purple solution. The solution was stirred for 1 hour and $AgSbF_6$ (153.6 mg, 0.45 mmol, 4.5 equiv) was then added. The addition of silver salt was done in a slight excess in order to make sure that all the bromide ions were removed. The solution turned into a yellow suspension. The stirring was then stopped and after 1 hour all the solid had settled down, the solution was filtered into a clean Schlenk flask. The remaining solid was washed with 2 mL of dry and degassed acetonitrile and the solution was then filtered into the Schlenk flask containing the previous filtrate. Into this dark brown filtrate, 2,2'-bipyridine (31.04 mg, 0.2 mmol, 2 equiv.) was added. The resulting orange solution was then stirred for another hour, and then concentrated until approximately 1 mL of the solution was left in the flask. Into the solution, 12 mL dry and degassed diethyl ether was then added, resulted in formation of a red oil. The solvent was then removed by filtration using a syringe filter and the resulting red oil was re-dissolved in 1 mL methanol. Dry and degassed diethyl ether (12 mL) was then added into the solution which led to formation of [**3**](SbF$_6$)$_2$ as a red solid. The solid was washed twice with diethyl ether, filtered and dried in vacuo. Yield: 178 mg, 0.189 mmol, 93%. ^{1}H-NMR (300 MHz, (CD$_3$)$_2$CO, RT) δ(ppm): 1.84 (m, 2H, S-C**H$_2$**), 2.26 (m, 2H, S-CH$_2$-C**H$_2$**-N), 5.07-5.13 (d, 2H, py-C**H$_2$**-N), 6.01-6.15 (d, 1H, py-C**H$_2$**-N), 7.28-10.00 (m, 40H, 16H from [**3**](SbF$_6$)$_2$, 24H from [Co(bpy)$_3$]$^{3+}$ species). IR (neat, cm^{-1}): 1700w, 1600m, 1573w, 1485w, 1471w, 1364w, 1318w, 1246w, 1163w, 1088w, 766s, 651vs. ESI-MS calcd. for [**3**](SbF$_6$)$^+$ *m/z* 708.0, found *m/z* 708.0, calcd. for [**3**]$^{2+}$ *m/z* 236.55, found *m/z* 236.6. Elemental analysis (%) for [**3**](SbF$_6$)$_2$·1.5H$_2$O, calcd. C, 29.66; H, 2.80; N, 7.21; found C, 29.59; H, 2.66; N, 7.13.

2.6. References

1. Paulsen, C. E. and Carroll, K. S. *Chem. Rev.* **2013**, 113 (7), 4633-4679.

2. Cramer, J. D. and Jarrett, J. T., *Methods in Enzymology*: *Radical SAM Enzymes*, 13, **2018**, Vol. 606, 363-388.
3. Poole, L. B. *Free Radical Biol. Med.* **2015**, 80, 148-157.
4. Sato, I., Shimatani, K., Fujita, K., Abe, T., Shimizu, M., Fujii, T., Hoshino, T. and Takaya, N. *J. Biol. Chem.* **2011**, 286 (23), 20283-20291.
5. Xiao, Z., La Fontaine, S., Bush, A. I. and Wedd, A. G. *J. Mol. Biol.* **2019**, 431 (2), 158-177.
6. Ueno, Y., Tachi, Y. and Itoh, S. *J. Am. Chem. Soc.* **2002**, 124 (42), 12428-12429.
7. Thomas, A. M., Lin, B.-L., Wasinger, E. C. and Stack, T. D. P. *J. Am. Chem. Soc.* **2013**, 135 (50), 18912-18919.
8. Ording-Wenker, E. C. M., van der Plas, M., Siegler, M. A., Bonnet, S., Bickelhaupt, F. M., Fonseca Guerra, C. and Bouwman, E. *Inorg. Chem.* **2014**, 53 (16), 8494-8504.
9. Ording-Wenker, E. C. M., van der Plas, M., Siegler, M. A., Fonseca Guerra, C. and Bouwman, E. *Chem. Eur. J.* **2014**, 20 (51), 16913-16921.
10. Gennari, M., Gerey, B., Hall, N., Pecaut, J., Collomb, M.-N., Rouzieres, M., Clerac, R., Orio, M. and Duboc, C. *Angew. Chem. Int. Ed.* **2014**, 53 (21), 5318-5321.
11. Wang, L., Reinhard, F. G. C., Philouze, C., Demeshko, S., de Visser, S. P., Meyer, F., Gennari, M. and Duboc, C. *Chem. Eur. J.* **2018**, 24 (46), 11973-11982.
12. Osako, T., Ueno, Y., Tachi, Y. and Itoh, S. *Inorg. Chem.* **2004**, 43 (21), 6516-6518.
13. Gennari, M., Brazzolotto, D., Yu, S., Pecaut, J., Philouze, C., Rouzieres, M., Clerac, R., Orio, M. and Duboc, C. *Chem. Eur. J.* **2015**, 21 (51), 18770-18778.
14. Itoh, S., Nagagawa, M. and Fukuzumi, S. *J. Am. Chem. Soc.* **2001**, 123 (17), 4087-4088.
15. Jiang, F., Siegler, M. A., Sun, X., Jiang, L., Fonseca Guerra, C. and Bouwman, E. *Inorg. Chem.* **2018**, 57 (15), 8796-8805.
16. Miessler, G. L., Fischer, P. J. and Tarr, D. A. *Inorganic Chemistry*. 5th ed.; 2014; p 696.
17. Sharpe, A. G. and Housecroft, C. E. *Inorganic Chemistry*. 4th ed.; Pearson Education Limited: 2012; p 1256.
18. Addison, A. W., Rao, T. N., Reedijk, J., Vanrijn, J. and Verschoor, G. C. *J. Chem. Soc., Dalton Trans.* **1984**, (7), 1349-1356.
19. Cowan, M. G., Olguin, J., Narayanaswamy, S., Tallon, J. L. and Brooker, S. *J. Am. Chem. Soc.* **2012**, 134 (6), 2892-2894.
20. Taylor, R. A., Lough, A. J. and Lemaire, M. T. *J. Mater. Chem.* **2016**, 4 (3), 455-459.
21. Furmeyer, F., Munzberg, D., Carrella, L. M. and Rentschler, E. *Molecules* **2020**, 25 (4)
22. Griffith, J. S. and Orgel, L. E. *Quarterly Reviews, Chemical Society* **1957**, 11 (4), 381.
23. Shimura, Y. and Tsuchida, R. *Bull. Chem. Soc. Jpn.* **1956**, 29 (3), 311-316.
24. Tsuchida, R. *Bull. Chem. Soc. Jpn.* **1938**, 13 (5), 388-400.
25. Tsuchida, R. *Bull. Chem. Soc. Jpn.* **1938**, 13 (6), 436-450.
26. Ashley, D. C. and Jakubikova, E. *Inorg. Chem.* **2018**, 57 (16), 9907-9917.
27. Jiang, F., Marvelous, C., Verschuur, A. C., Siegler, M. A., Teat, S. J. and Bouwman, E. *Inorg. Chim. Acta* **2022**, 120880.
28. Irving, H. and Mellor, D. H. *J. Chem. Soc* **1962**, (DEC), 5237-&.
29. Makrlík, E. and Vaňura, P. *Colloids Surf., A* **1992**, 68 (3), 195-197.
30. Strohalm, M., mMass - Open Source Mass Spectrometry Tool. www.mmass.org
31. Sheldrick, G. M. *Acta Crystallogr. Sect. A: Found. Crystallogr.* **2008**, 64, 112-122.
32. Spek, A. L. *Acta Crystallogr. Sect. C: Cryst. Struct. Commun.* **2015**, 71 (Pt 1), 9-18.
33. Spek, A. L. *Acta Crystallogr. Sect. D. Biol. Crystallogr.* **2009**, 65 (2), 148-155.
34. ADF2017.107. SCM Theoretical Chemistry, Vrije Universiteit: Amsterdam, The Netherlands, www.scm.com
35. Swart, M., Ehlers, A. W. and Lammertsma, K. *Mol. Phys.* **2004**, 102 (23-24), 2467-2474.
36. Van Lenthe, E. and Baerends, E. J. *J. Comput. Chem.* **2003**, 24 (9), 1142-1156.
37. Van Lenthe, E., Baerends, E. J. and Snijders, J. G. *J. Chem. Phys.* **1994**, 101 (11), 9783-9792.